Ellipsoidal Relaxation of Deformed Vesicles: Supplemental Material

Miao Yu,[1] Rafael B. Lira,[2,3] Karin A. Riske,[3] Rumiana Dimova,[2] and Hao Lin[1]

[1]*Department of Mechanical and Aerospace Engineering, Rutgers, The State University of New Jersey, 98 Brett Road, Piscataway, NJ 08854, USA*

[2]*Department of Theory and Bio-Systems, Max Planck Institute of Colloids and Interfaces, Science Park Golm, 14424 Potsdam, Germany*

[3]*Department of Biophysics, Federal University of São Paulo, BR-04044020 Sao Paulo, Brazil*

(Dated: August 4, 2015)

Abstract

Theoretical analysis and experimental quantification on the ellipsoidal relaxation of vesicles are presented. The current work reveals the simplicity and universal aspects of this process. The Helfrich formula is shown to apply to the dynamic relaxation of moderate-to-high tension membranes, and a closed-form solution is derived which predicts the vesicle aspect ratio as a function of time. Scattered data are unified by a timescale, which leads to a similarity behavior, governed by a distinctive solution for each vesicle type. Two separate regimes in the relaxation are identified, namely, the "entropic" and the "constant-tension" regime. The bending rigidity and the initial membrane tension can be simultaneously extracted from the data/model analysis, posing the current approach as an effective means for the mechanical analysis of biomembranes.

PACS numbers: 82.70.Uv, 47.63.mf, 87.16.D-, 87.85.G-

S1. BASIC THEORY

Our basic theory for the ellipsoidal relaxation of vesicles derives from that of Seifert [1] (denoted as S99 below), and a brief account is given here. In the theory, the vesicle has a quasi-spherical shape which conserves both volume and surface area. By considering the Stokes flow both interior and exterior to the vesicle, and interfacial continuity conditions for both velocity and stress, a Langevin equation is derived for each mode of the spherical harmonics (Eq. (50) in S99):

$$\partial_t u_{l,m} = S - \frac{\kappa}{\mu r_0^3} E_l F_l u_{l,m} + \zeta_{l,m}. \tag{S1}$$

Here $u_{l,m}$ is the amplitude of a spherical harmonics of mode $(l,\ m)$, S includes the effects of an external driving force (e.g., a shear flow), κ is the membrane bending rigidity, μ is the viscosity (temporarily assumed to be the same for both the interior and exterior in the above equation), r_0 is the vesicle radius in the spherical state, and $\zeta_{l,m}$ is thermal noise. The coefficients E_l and F_l are given by

$$E_l = (l+2)(l-1)\left[l(l+1) + \frac{r_0^2}{\kappa}\Gamma\right],$$

$$F_l = \frac{l(l+1)}{4l^3 + 6l^2 - 1},$$

where Γ is the isotropic membrane tension. In relaxation in the absence of an external driving flow, we can set $S = 0$. For each mode, we decompose the total amplitude $u_{l,m}$ into a "mean" component that is apparently observable, $\bar{u}_{l,m}$, and a component due to thermal fluctuation, $u_{l,m}^{'}$,

$$u_{l,m}(t) = \bar{u}_{l,m}(t) + u_{l,m}^{'}(t).$$

Their governing equations are respectively,

$$\partial_t \bar{u}_{l,m} = -\frac{\kappa}{\mu r_0^3} E_l F_l \bar{u}_{l,m}, \tag{S2}$$

and

$$\partial_t u_{l,m}^{'} = -\frac{\kappa}{\mu r_0^3} E_l F_l u_{l,m}^{'} + \zeta_{l,m}. \tag{S3}$$

We assume that $u_{2,0}$ is the only mode controlling the apparent (macroscopically observable) vesicle shape - this assumption is supported by many direct experimental observations [2, 3], and further justification is given in Section S4. By setting $(l, m) = (2, 0)$ in Eq. (S2) we arrive at a governing equation for $\bar{u}_{2,0}$,

$$\partial_t \bar{u}_{2,0} = -\frac{24\kappa}{55\mu r_0^3}\left(\frac{r_0^2}{\kappa}\Gamma + 6\right)\bar{u}_{2,0}. \tag{S4}$$

Next, the membrane tension needs to be determined via the total area constraint,

$$\Delta + \Delta_f = \Delta_{tot}. \tag{S5}$$

Here Δ is the dimensionless "systematic" deformation which corresponds to the contributions of $\bar{u}_{l,m}$, defined as

$$\Delta = \frac{A}{4\pi r_0^2} - 1,$$

where A is the "apparent" surface area of the membrane. If only $\bar{u}_{2,0}$ is present, then we have

$$\Delta = \frac{1}{2\pi}|\bar{u}_{2,0}|^2.$$

Δ_f and Δ_{tot} are also similarly defined: Δ_f is the dimensionless area stored in the (microscale) thermal fluctuations, and Δ_{tot} is the total "excess" area which is a constant for a given vesicle (membrane). Note that our definition differs by a factor of 4π when compared with that in S99 (*c.f.* Eq. (71) therein). We temporarily assume that all fluctuation has evolved to the so-called "stationary" state, namely,

$$\lim_{t\to\infty}\langle|u'_{l,m}|^2\rangle = \frac{k_B T}{\kappa E_l}. \tag{S6}$$

This assumption will be carefully justified below. The area stored in each mode is

$$\Delta_{l,m} = \frac{k_B T}{8\pi\kappa}\frac{1}{l(l+1) + \Gamma r_0^2/\kappa}. \tag{S7}$$

Summing over the modes leads to an expression for Δ_f,

$$\Delta_f = \frac{k_B T}{8\pi\kappa}\sum_{l\geq 2}\frac{2l+1}{l(l+1) + \Gamma r_0^2/\kappa}. \tag{S8}$$

Using an integration to approximate the summation in (S8), we obtain

$$\Delta_f = \frac{k_B T}{8\pi\kappa}\ln\frac{l_{max}^2 + l_{max} + \Gamma r_0^2/\kappa}{6 + \Gamma r_0^2/\kappa}, \tag{S9}$$

where $l_{max} = r_0/d$ and d is the membrane thickness.

We focus on the so-called "entropic" regime as noted by S99 (Eq. (74) therein),

$$6 \ll \frac{\Gamma r_0^2}{\kappa} \ll l_{max}^2. \tag{S10}$$

For the current study, the isotropic tension Γ is self-consistently determined to be $\sim 10^{-6}$ N/m (see Tables S2-S5 in Section S4). Using $\kappa \sim 10^{-19}$ J, and $r_0 \sim 20\ \mu$m, we obtain

$$\frac{\Gamma r_0^2}{\kappa} \sim 4 \times 10^3.$$

On the other hand, using $d \sim 5$ nm results in $l_{max} \sim 4 \times 10^3$ and therefore $l_{max}^2 \sim 10^7$. These estimates demonstrate that the constraint (S10) is well-satisfied, so that Eq. (S9) becomes

$$\Delta_f \approx \frac{k_B T}{8\pi\kappa} \ln \frac{l_{max}^2}{\Gamma r_0^2/\kappa}. \tag{S11}$$

Eq. (S11) effectively leads to the constitutive relation in the "entropic" regime. Substituting (S11) into (S5) we obtain

$$\Gamma = \frac{\kappa}{d^2} \exp\left(-\frac{8\pi\kappa\Delta_{tot}}{k_B T}\right) \exp\left(\frac{8\pi\kappa\Delta}{k_B T}\right). \tag{S12}$$

If we define the initial tension, Γ_0, as the isotropic membrane tension when the systematic (apparent) deformation Δ is zero, namely, when the vesicle is in the relaxed spherical state, from Eq. (S12) we have,

$$\Gamma_0 = \frac{\kappa}{d^2} \exp\left(-\frac{8\pi\kappa\Delta_{tot}}{k_B T}\right). \tag{S13}$$

When applying the model, either Γ_0 or Δ_{tot} needs to be specified, and the other can be calculated according to Eq. (S13). Substituting (S13) into (S12) we arrive at

$$\Gamma = \Gamma_0 \exp\left(\frac{8\pi\kappa\Delta}{k_B T}\right). \tag{S14}$$

This equation is none but the Helfrich model, or Eq. (3) in the main text. In fact, per (S10), the Helfrich model is an excellent approximation to the original equation (S5) except for extremely high or low isotropic membrane tensions.

We have yet to justify the "stationary" assumption for $u'_{l,m}$, namely, Eq. (S6). We realize that this assumption predicates that the Helfrich formula (S14) is an "equilibrium" formula, which is only valid when given sufficient time to establish the stationary state. Indeed, most of the extensive experimental data supporting the Helfrich formula were also obtained when the membrane was in an equilibrated condition (e.g., in stationary deformed state via micropipette aspiration or AC field electrodeformation) [4–6]. However, here we demonstrate that the Helfrich formula is accurate even when the membrane is not in equilibrium such as during shape relaxation, provided that the tension Γ is sufficiently high.

First, according to Eqs. (S2, S3) we realize that the relaxation timescale for both $\bar{u}_{l,m}$ and $u'_{l,m}$ is

$$\tau_{l,m} = \frac{\mu r_0^3}{\kappa E_l F_l}. \tag{S15}$$

Indeed, integrating (S3) yields a formal solution for $u'_{l,m}(t)$,

$$u'_{l,m}(t) = \exp[-(\kappa/\mu r_0^3)E_l F_l t] \left(\int_0^t \mathrm{d}t' \left\{ \exp[(\kappa/\mu r_0^3)E_l F_l t']\zeta_{l,m}(t') + u'_{l,m}(0) \right\} \right).$$

If $\Gamma r_0^2/\kappa \gg l(l+1)$, then $\tau_{l,m} \sim l^{-1}$; otherwise $\tau_{l,m} \sim l^{-3}$. Therefore, for the higher modes, both the mean and the fluctuation quickly evolve to equilibrium (sphericity) and stationary correlation, respectively.

Note that subtly, these states are "quasi-stationary", as in relaxation, E_l also changes with time due to the time-dependence of Γ. The latter changes along with $u_{2,0}$, on a much greater timescale of $\tau_{2,0}$. Therefore as Γ "slowly" evolves, the higher-mode fluctuations always adapt "instantaneously" to a correspondingly evolving quasi-stationary state characterized by Eq. (S6). This situation is analogous to a moving piston in a chamber of ideal gas: if the piston moves sufficiently slowly, then the system is constantly in thermal quasi-equilibrium, due to the fact that the equilibrium process is comparatively rapid.

For a lower mode such as $u_{2,0}$ (ellipsoidal), the fluctuation converges to the stationary correlation on the same timescale of the apparent shape relaxation. This would seemingly violate the *ansatz* of our analysis, that all fluctuations are always in a stationary state quantified by (S6). Consequently, it would appear that (S8) and (S9) are no longer valid as $\Delta_{l,m}$ for the lower modes are not accounted for accurately due to deviation from the stationary state.

However, the following consideration restores the validity of (S8) and hence the accuracy of the Helfrich formula. We re-write the fluctuation area as

$$\Delta_f = \Delta_L + \Delta_H,$$

where

$$\Delta_L = \frac{k_B T}{8\pi\kappa} \sum_{l=2}^{l_c} \frac{2l+1}{l(l+1) + \Gamma r_0^2/\kappa} \tag{S16}$$

accounts for all modes with $l \leq l_c$, and

$$\Delta_H = \frac{k_BT}{8\pi\kappa} \sum_{l=l_c+1}^{l_{max}} \frac{2l+1}{l(l+1)+\Gamma r_0^2/\kappa} \approx \frac{k_BT}{8\pi\kappa} \ln\left(\frac{l_{max}^2 + l_{max} + \Gamma r_0^2/\kappa}{(l_c+1)(l_c+2)+\Gamma r_0^2/\kappa}\right)$$

accounts for all higher modes modes with $l > l_c$. Here we choose $l_c = 20$, because using (S15) and $\Gamma r_0^2/\kappa = 4 \times 10^3$, we find

$$\frac{\tau_{20,m}}{\tau_{2,m}} \approx 0.077.$$

Therefore, for $l > l_c$ we can assume that the modes relaxes sufficiently fast and are always in thermal equilibrium (the stationary state).

On the other hand, the values for Δ_L, Δ_H, and Δ_f for Γ ranging from 10^{-8} to 10^{-3} N/m are tabulated in Table S1. Evidently, the contribution of Δ_L to Δ_f is of several percent at most for $\Gamma \gtrsim 10^{-7}$ N/m, and negligibly small for $\Gamma \gtrsim 10^{-6}$ N/m. Furthermore, although in the non-stationary state the exact value of $\Delta_{l,m}$ may differ from Eq (S7), its magnitude is determined by $\zeta_{l,m}$ and cannot deviate significantly. Combining these considerations, we conclude that Δ_f as given by (S8) is still sufficiently accurate in a dynamic, shape-relaxation process. Hence following Eqs. (S5-S14), the Helfrich formula is also accurate. We therefore conclude that although the Helfrich formula is derived assuming that all fluctuations are in thermal equilibrium, it is still a highly accurate constitutive relation for shape relaxation with sufficiently high isotropic membrane tension, due to the fact that the lower modes contribute negligibly to the total area stored in the thermal fluctuations. On the other hand, the Helfrich formula eventually loses accuracy when Γ decreases (or $\Gamma r_0^2/\kappa$ approaches 6), as for these cases the lower modes become more significant in their contributions to Δ_f. In this case, the Langevin equation for the fluctuations (S3) needs to be numerically solved to properly calculate the areas.

Finally, Eq. (S4) is converted to Eq. (1) in the main text by considering $u_{2,0} = \frac{4}{3}\sqrt{\frac{\pi}{5}}\epsilon$,

$$\frac{\mathrm{d}\epsilon}{\mathrm{d}\tau} = -\frac{24}{55}\epsilon \exp\left(\frac{8\pi\kappa\Delta}{k_BT}\right),$$

where we have used $\Gamma r_0^2/\kappa \gg 6$. While the above equation is derived assuming $\mu_i = \mu_e = \mu$, the effects of differing viscosities can be accounted for following, e.g., Schwalbe et al. [7]. The final result is Eqs. (1, 2) in the main text.

Note that the final ODE is autonomous, since Δ depends only on ϵ. This means if $y(\tau)$ is a solution for the initial condition $\epsilon(\tau = 0) = \epsilon_0$, then the solution for an arbitrary

Γ (N/m)	$\Delta_L \times (8\pi\kappa/k_BT)$	$\Delta_H \times (8\pi\kappa/k_BT)$	$\Delta_f \times (8\pi\kappa/k_BT)$	Δ_L/Δ_f
10^{-8}	2.40	10.4	12.8	0.187
10^{-7}	0.734	9.85	10.6	6.93×10^{-2}
10^{-6}	0.103	8.19	8.29	1.25×10^{-2}
10^{-5}	1.09×10^{-2}	5.98	5.99	1.81×10^{-3}
10^{-4}	1.11×10^{-3}	3.71	3.71	2.94×10^{-4}
10^{-3}	1.09×10^{-4}	1.61	1.61	6.79×10^{-5}

TABLE S1: Calculated values of Δ_L, Δ_H, and Δ_f for various values of membrane tension, Γ. For these calculations we set r_0=20 μm and κ=10^{-19} J. Evidently the contribution of the lower modes to the area stored in the fluctuation is small for $\Gamma \gtrsim 10^{-7}$ N/m.

initial condition, $\epsilon(\tau = 0) = \epsilon_1$, can be obtained via a simple translation, $y(\tau + \tau_1)$, where $\tau_1 = y^{-1}(\epsilon_1)$. Thus for such system, translation can be used to collapse solutions with varying initial condition, such as in the main text.

A comparison between vesicle and droplet relaxation is appropriate here. In the limit of $\Delta \to 0$, we have $\Gamma/\Gamma_0 \to 1$, and the so-called constant-tension regime is reached as described in the main text. The simplified governing equation is

$$\frac{\mu_e r_0}{\Gamma_0}\frac{\mathrm{d}\epsilon}{\mathrm{d}t} = -C\epsilon, \quad C = \frac{24}{32 + 23\mu_r}, \tag{S17}$$

which can be compared with that of ellipsoidal droplet relaxation [8],

$$\frac{\mu_e r_0}{\gamma}\frac{\mathrm{d}\epsilon}{\mathrm{d}\tau} = -C_{drop}\epsilon, \quad C_{drop} = \frac{40(\mu_r + 1)}{(2\mu_r + 3)(19\mu_r + 16)}. \tag{S18}$$

Comparing Eqs. (S17) and (S18), we observe that we only need to replace the initial tension Γ_0 with the surface tension for the droplet, γ; and the coefficient C with C_{drop} to arrive at the droplet equation from the vesicle counterpart. The main difference, namely, C and C_{drop}, results from the fact that area incompressibility is enforced for vesicles; whereas for droplets, continuity of the tangential fluid stress is prescribed instead. Nevertheless, the two equations are in close quantitative agreement. For example, for $\mu_r = 1$, $C = 0.436$, and $C_{drop} = 0.457$. The relative difference is less than 5%.

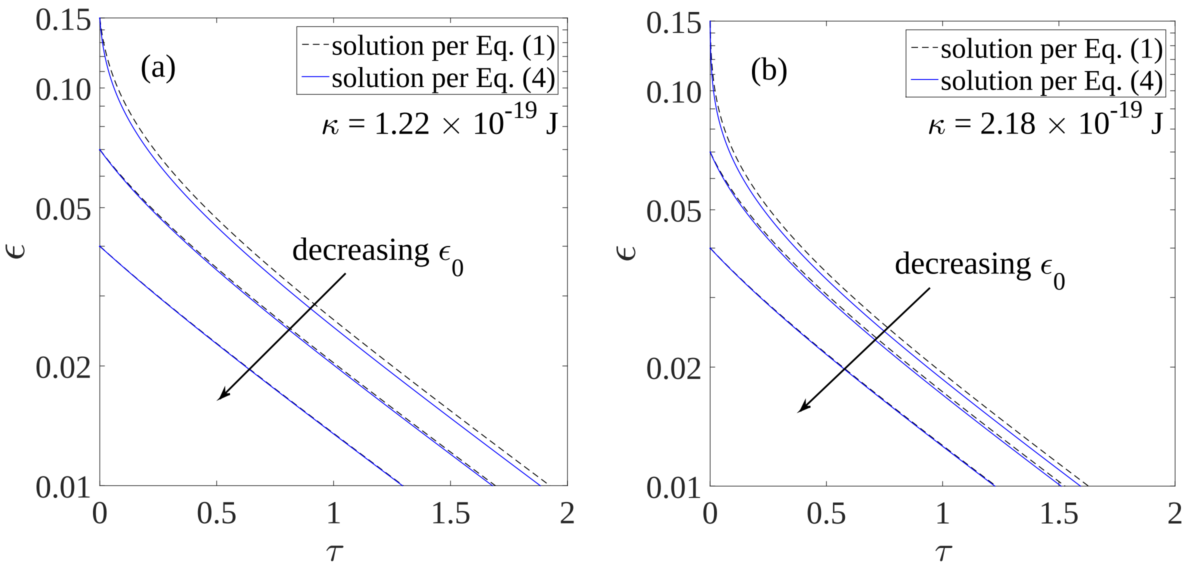

FIG. S1: Comparison between numerical solutions to Eq. (1) (dashed) and Eq. (4) (solid). (a) $\kappa = 1.22 \times 10^{-19}$ J (POPC); ϵ_0= 0.04, 0.07 and 0.15, respectively. (b) $\kappa = 2.18 \times 10^{-19}$ J (POPC with 30% cholesterol); ϵ_0= 0.04, 0.07 and 0.15, respectively.

S2. ACCURACY OF EQ. (4) AND MEMBRANE DISCHARGING EFFECTS

In the main text, we have derived a closed-form solution of Eq. (1) by approximating the apparent area increase, Δ, with the leading-order term in its Taylor expansion, namely, $\Delta \cong \frac{8}{45}\epsilon^2$. Naturally, such expansion loses accuracy when ϵ increases sufficiently in magnitude. Here we briefly examine the accuracy of Eq. (4) as an approximate solution to Eq. (1), the original governing equation.

We examine two cases, namely, $\kappa = 1.22$ and 2.18×10^{-19} J, which correspond to the bending rigidity of POPC and POPC with 30% cholesterol, respectively. For initial conditions, we pick $\epsilon_0 = 0.04$, 0.07, and 0.15, respectively. Solutions are obtained from numerically solving Eq. (1), and are plotted in Fig. S1 as dashed lines. Solutions using Eq. (4) are also shown as solid lines by directly using the "expint" function (exponential integral) from MATLAB. We observe that indeed the approximate solution (4) follows closely the original solution using (1), although the differences are more visible for $\epsilon_0 = 0.15$, for both cases.

Figure S2 further quantifies these differences. Here the maximum error in ϵ for each case is plotted as a function of the initial condition, ϵ_0. For $\kappa = 1.22 \times 10^{-19}$ J (POPC), the maximum difference increases to 0.005 for $\epsilon_0 = 0.15$. For $\kappa = 2.18 \times 10^{-19}$ J (POPC with

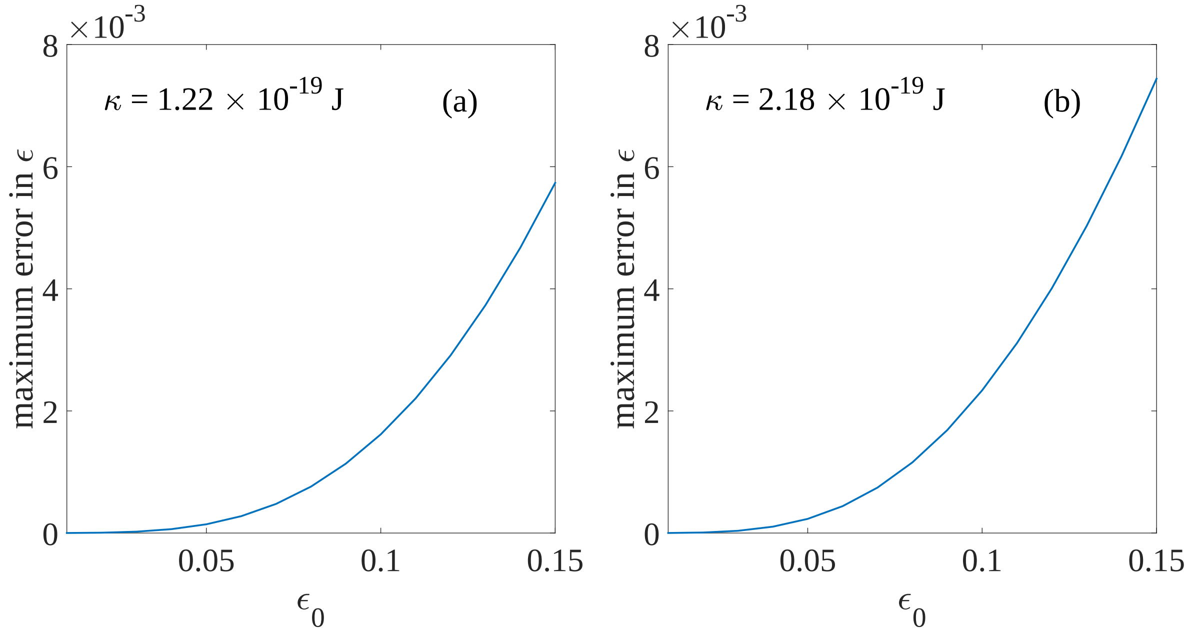

FIG. S2: Maximum error of ϵ between numerical solutions to Eq. (1) and Eq. (4), plotted as a function of ϵ_0. (a) $\kappa = 1.22\times10^{-19}$ J (POPC). (b) $\kappa = 2.18\times10^{-19}$ J (POPC with 30% cholesterol).

30% cholesterol), the maximum difference is observed to be less than 0.008 for $\epsilon_0 = 0.15$. For both cases, the maximum difference is only a few percent of the value of ϵ_0. Overall, these results suggest that Eq. (4) serves as a good and convenient approximation solution to Eq. (1) for parametric ranges of our interest.

Another effect that we need to carefully evaluate, and that is particular to the current deformation technique, is the membrane discharging effect. In the current work, we assume that once the electric field ceases, the electrostatic stress (the external driving force) disappears instantaneously and relaxation begins. In actuality, the vesicle membrane has a finite capacitance, and discharges on a well-known timescale [2, 3]

$$t_{mm} = \frac{r_0 C_{mm}}{\sigma_{in}} \left(1 + \frac{\sigma_r}{2}\right), \tag{S19}$$

where $C_{mm} \sim 0.08$ F/m^2 is the membrane capacitance, σ_{in} and σ_{out} denote the intra- and extra-vesicular electrical conductivity, respectively, and $\sigma_r = \sigma_{in}/\sigma_{out}$ is their ratio. For the cases in the current manuscript, using $r_0 = 20$ μm, $\sigma_{in} = 6$ μS/cm, and σ_{out} =2 μS/cm (see Section S3), we obtain a discharging timescale of 0.8 ms. This timescale is much smaller than the relaxation timescale, namely, t_D (Eq. (1) in the main text). The latter is on the order of tens of ms (see Fig. S5 below). Furthermore, the effects caused by the residual electrostatic stress due to discharging is in general negligible as we demonstrate below. We restore the effect of the electric field during membrane discharging via the S-term in Eq. (S1) [3],

$$t_D \frac{\partial \epsilon}{\partial t} = \frac{3}{32+23\mu_r} \frac{\sigma_r^2 - 16}{(\sigma_r+2)^2} \left(\frac{\epsilon_w E_0^2 r_0}{\Gamma_0} \right) \bar{V}_{mm} - \frac{24}{32+23\mu_r} \frac{\Gamma}{\Gamma_0} \epsilon, \tag{S20}$$

$$\bar{V}_{mm} = \frac{3}{2}(1 - e^{-t_p/t_{mm}}) e^{-t/t_{mm}}. \tag{S21}$$

Here ϵ_w is the permittivity of the buffer solution (taken to be that of water), E_0 is the applied field strength, t_p is pulse duration, and $\bar{V}_{mm}$ is a dimensionless transmembrane potential which demonstrates a rapid, exponential decay on the timescale of t_{mm} due to discharging. Equation (S20) is solved numerically and compared with the solution with Eq. (1) in the main text. The results for a few typical parametric settings are shown in Fig. S3. Evidently, the effects caused by discharging is negligible, simply due to the fact that for the parametric range we consider, the electrostatic forcing term in (S20) has a small amplitude when compared with the term controlling relaxation (the second term on the RHS of that equation). In addition, this term also decays exponentially on a short timescale of t_{mm}, as with typical capacitive discharging.

S3. EXPERIMENTAL MATERIALS AND METHODS

Preparation of giant unilamellar vesicles

Giant unilamellar vesicles (GUVs) of 1-palmitoyl-2-oleoyl-sn-glycero-3-phosphocholine (POPC) with 0, 10, 20, and 30% cholesterol (by mole fraction) were prepared following the classical electroformation method described in Angelova and Dimitrov [9]. POPC and cholesterol (Avanti Polar Lipids, Alabaster, AL) were diluted in chloroform and mixed at given molar ratios. For electroformation, 8-10 μL of a 3-mM lipid solution in chloroform were spread on a pair of conductive ITO glasses. Solvent was evaporated by a stream of N_2 for 5 min (dessication under vacuum for 2 hours yielded the same results). The glasses were sandwiched using a 1-mm Teflon spacer forming a chamber with $\sim$ 1.5 mL of volume and coupled to a function generator. An AC field of 1 V at 10 Hz was applied and a 0.05-M sucrose solution was added to the chamber. Vesicles were allowed to grow for 1 h at room temperature. After vesicle formation was observed, the vesicle solution was removed

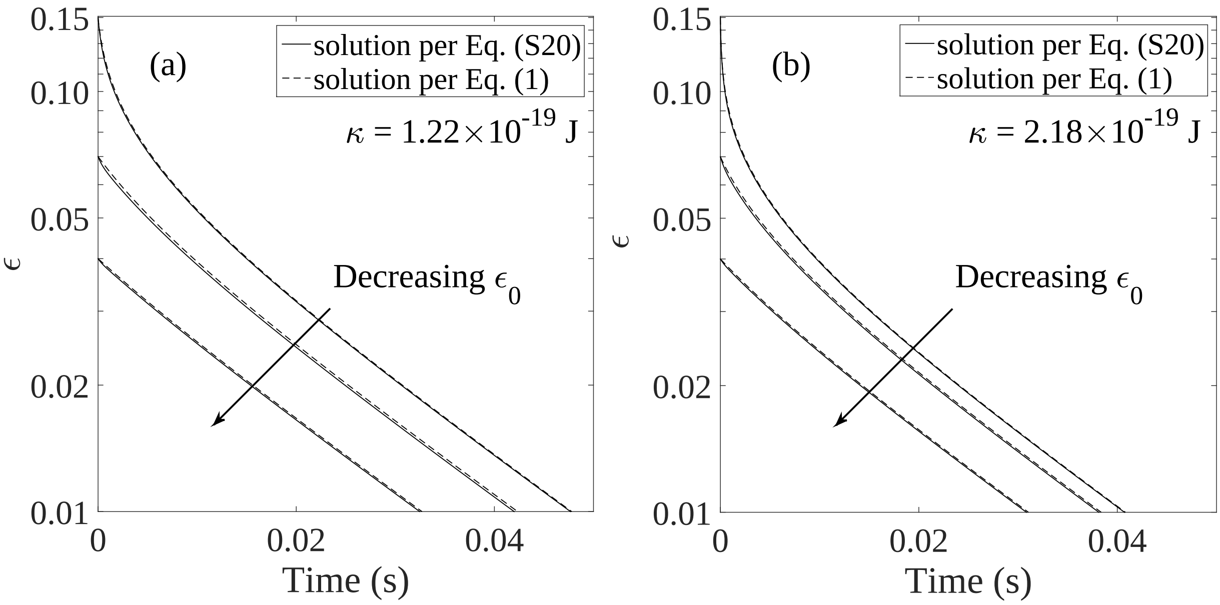

FIG. S3: Comparison between numerical solutions to Eq. (S20) (with discharging effect) and Eq. (1) (without discharging effect), for ϵ_0= 0.04, 0.07 and 0.15, respectively. (a) $\kappa = 1.22 \times 10^{-19}$ J (POPC). (b) $\kappa = 2.18 \times 10^{-19}$ J (POPC with 30% cholesterol). In both figures, the strengths and the lengths of the applied electric pulses are (50V, 50 μs), (50V, 100 μs), and (80V, 100 μs), corresponding to ϵ_0= 0.04, 0.07, and 0.15, respectively. These protocols are chosen as they typically resulted in similar values of ϵ_0 in our experiments.

from the chamber and diluted into a 0.05-M glucose solution. To avoid osmotic pressure effects, the osmolarities of the sucrose and glucose solutions were carefully matched using a cryoscopic osmometer Osmomat 030 (Gonotec, Berlin, Germany). An inverted microscope Axiovert 135 (Zeiss, Jena, Germnay) equipped with a 20× phase contrast lens was used to visualize the GUVs, with image sequences acquired at 20,000 frames per second by a high-speed digital camera HG-100K (Redlake, San Diego, CA). Further details can be found in previous works by two of us (KAR and RD) [2, 10].

Pulse protocols for electrodeformation

The vesicle suspension was placed into an observation chamber with built-in electrodes (Eppendorf, Hamburg, Germany) where DC pulses were applied from a Multiporator (Eppendorf, Hamburg, Germany) to induce electrodeformation. The distance between the electrodes was 500 μm. The voltages applied across the electrodes were chosen among the values of 50 V, 80 V, and 100 V. The pulse length varied between 50 μs and 300 μs. Intra- and extra-vesicular electrical conductivities were 6 and 2 μS/cm, respectively. Details of pulse information for each experiment are listed in Tables S2-S6.

Intra- and extra-vesicular viscosities

To compare experimental results with our theory, it is necessary to know the values of the intra- and extra-vesicular viscosities. In this study, viscosity values are obtained from linear extrapolation of previous measurements of sucrose and glucose solutions [11]. For sucrose solution, the viscosities for molar concentrations of 0.186 M and 0.120 M were reported to be 1.179 mPa·s and 1.215 mPa·s, respectively. For glucose solution, the viscosities for molar concentrations of 0.169 M and 0.225 M were reported to be 1.083 mPa·s, and 1.113 mPa·s, respectively. By linear extrapolation, the intra-vesicular (0.05 M sucrose) and the extra-vesicular (0.05 M glucose) viscosities of the current experiments are calculated to be 1.253 and 1.019 mPa·s, respectively. These values are used in the theoretical models and data analysis.

S4. DATA ANALYSIS

Images are analyzed to extract the two-dimensional vesicle contour, as well as to extract e or ϵ, following the approach developed by one of us (RD, [6]). Importantly, a Fourier analysis of the shape contour does reveal that the P_2 (ellipsoidal) mode dominates. The spectral analysis assumes

$$r = r_0 \left(1 + \sum_{l \geq 2} [a_l \cos(l\theta) + b_l \sin(l\theta)] \right).$$

Here the $l = 1$ mode corresponds to translation and is not included. The amplitude for each mode is $\sqrt{a_l^2 + b_l^2}$, and the amplitude for $l = 2$ is related to the aspect ratio e as

$$e = \frac{1 + \sqrt{a_2^2 + b_2^2}}{1 - \sqrt{a_2^2 + b_2^2}}.$$

Two typical cases are shown in Fig. S4, in which the amplitudes for the first three modes are presented. Evidently, P_2 is the only mode which has an appreciable contribution to the apparent vesicle shape.

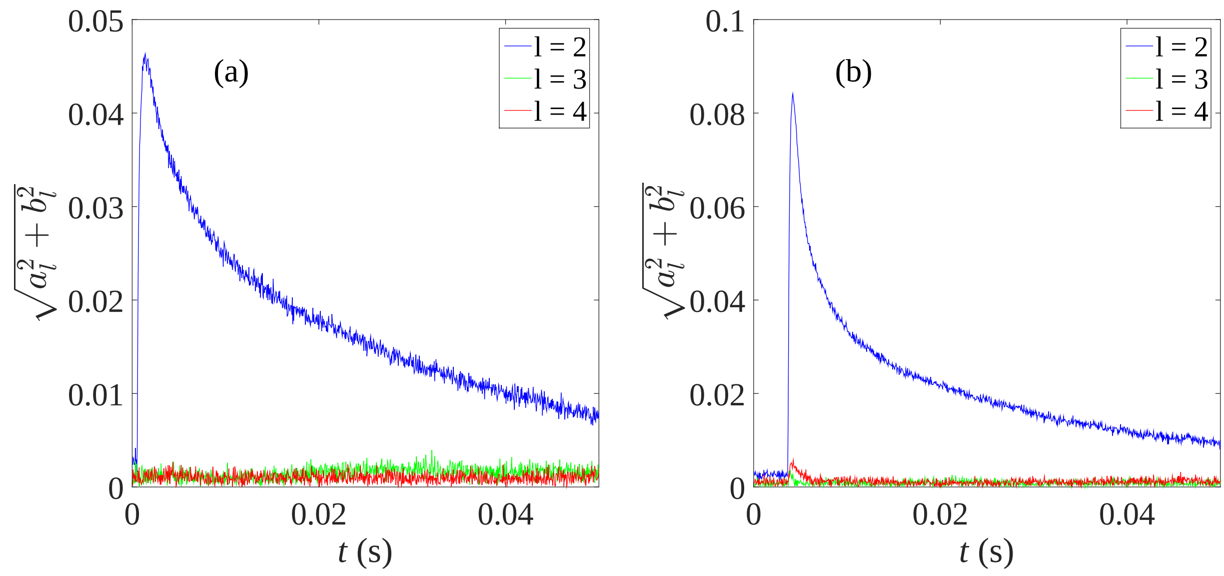

FIG. S4: Exemplary amplitude evolution of $l = 2$, 3 and 4 modes during relaxation. (a) Vesicle #4, POPC with 30% cholesterol (Table S5). (b) Vesicle #7, POPC (Table S2).

This result is also straightforward to appreciate from a theoretical point of view. First, for a smooth contour, the amplitude of the spherical harmonics decays exponentially with the mode number l (known as spectral convergence). Second, the relaxation time decreases approximately with l^{-1} or l^{-3} (see Eq. (S15)). Combining these considerations, the higher modes not only have smaller amplitudes to begin with, but also decay more rapidly, leaving P_2 to dominate.

In the main text, we present results on the extraction of two important parameters, namely, κ and Γ_0. Below, we present three different approaches for the same purpose and demonstrate that they lead to consistent values of κ and Γ_0 within data uncertainty. All obtained values are tabulated in Tables S2-S6. For all cases, only data above $\epsilon = 0.015$ are used as we have explained in the main text. Other pertinent values, that is, r_0, μ_i, and μ_e, are measured or obtained from linear extrapolation as discussed above.

The first approach is termed “Method A”. In this case, for each individual vesicle, κ and Γ_0 are identified by minimizing the root-mean-square (RMS) error between the data and solution (4). The mean and standard deviations (STD) are also calculated. Shown in the tables are also the mean RMS error which is defined as the average of the RMS error over all vesicles in each table, and the values of R^2, the coefficient of determination.

The second is termed “Method B”. In this case, we assume that κ remains the same for all vesicles of the same type, whereas Γ_0 varies among them. For each value of κ, Γ_0 is identified for each vesicle so as to minimize the error; a mean error is obtained by averaging over all vesicles in the group. This mean error changes as κ changes, and an "optimal" value is obtained by finding its minimum.

The third is termed "Method C". In this case, we take advantage of the separation of the entropic and constant-tension regimes: κ and Γ_0 are extracted from these two regimes, respectively. First, we examine the data, and determine a threshold value for ϵ below which the constant-tension regime is reached. The determination of this threshold value is empirical: on a semi-logy scale, we "cut-off" the section of data that appears to be linear. The cut-off value is 0.025 for all cases studied here. This value is conservatively low to ensure constant tension behavior. The data is then fitted with a least-square line on a semi-logy scale. From the theory, the slope of the line, s, is given by:

$$s = C/t_D = C\Gamma_0/\mu_e r_0.$$

Knowing r_0, μ_i, and μ_e allows us to extract Γ_0 from the values of s. Note that in the constant-tension regime, the data trend is controlled by Γ_0, and κ has minimal effects. In the next step, once Γ_0 is determined, κ can be identified by minimizing the error between the solution (4) and the entire section of data, both entropic and constant-tension regimes included. In this case, the determination of κ is mostly via data in the entropic regime, as the constant-tension regime is not sensitive to the changes in κ. We remark that Method C is the most physical approach, as we harness the separation of regimes, and for each regime, instead of a two-parameter fitting, only a one-parameter fitting is performed.

Results from the first 4 groups in Fig. 3 in the main text are shown in Tables S2-S5. Each table lists detailed parameters and analysis of a single vesicle type, including the pulsing parameters, r_0, κ and Γ_0 from Methods A-C, and error analysis. Here we will introduce results on POPC, and other vesicle types follow a similar description.

Table S2 shows that for POPC, the bending rigidity κ extracted from Method A, B, and C are 1.14 ± 0.23, 1.20, and 1.00×10^{-19} J, respectively. Both the average value and STD from Method A are presented, whereas for B and C, κ is assumed to be the same across all cases. We see that all values are consistent and within 20% of deviation from each other.

More importantly, the mean error (M.E.) for each method is also evaluated. For this calculation, we first compute the RMS error between the theoretical prediction and the data in terms of ϵ, which is subsequently averaged among the vesicles in each group to obtain the M.E. The resulting values are 0.0025, 0.0027, and 0.0043, respectively. We see that in terms of accuracy, Method A is comparable with B, and are both appreciably better than that of Method C. This result is not surprising, as even though Method C is the most "physical" approach harnessing regime separation, Method A and B have better performance due to the fact that the error of fitting is minimized in the two-parameter phase space of κ and Γ_0, rather than in two steps as in Method C. Based on these evaluations, we choose to use Method B for the results presented in the main text, for the following reasons. First, the accuracy of this method is comparable with that of Method A, the best numerical fitting method since both κ and Γ_0 are "optimized" for each individual case (see also Tables S3-S5). Second, as each vesicle type is made with identical membrane composition, it is reasonable to assume a fixed κ value. Indeed, this assumption is supported by the result of Method A, which demonstrates a small STD from the analysis of individual cases. Furthermore, designating a constant κ for each vesicle type allows us to unite all data with a single solution such as shown in the main text. This approach provides a powerful and simple way to dissect the physics and behavior of vesicle relaxation. On the other hand, one can follow Method A if the primary interest is to extract properties of individual vesicles.

In Table S6, we present the analysis and information on the last group shown in Fig. 3 of the main text. Electroporation obviously resulted from the higher voltage and longer pulse duration when compared with other cases, which engendered a supercritical transmembrane potential for membrane permeabilization [2, 12].

Finally, Figs. S5a-S5e alternatively present the data in Tables S2-S6 on a linear scale for ϵ. Figure S5f presents the data in Fig. 3 in the main text, also on a linear scale. Fig. S6 presents the electroporated vesicles on a logarithmic scale. The vesicle are the same as those in Fig. 3 in the main text, but a greater range in ϵ is shown. The dashed line is a global fit for all 4 vesicles.

We remark that during the analysis we discard all data below $\epsilon = 0.015$, and we have done so consistently across all cases to avoid noise contamination of the analysis. This threshold is conservative, and in cases when the noise is less prominent, we can indeed relax the threshold and adopt lower cut-off values for ϵ. However, doing so will not appreciably alter the results, primarily because this part of the data is well within the "constant-tension" regime, in which the data exhibits a linear behavior between $\ln(\epsilon)$ and time. Extending the data simply extends the linearity. Fig. S7 demonstrates this idea with vesicle #4 of POPC with 30% cholesterol. In this case, a new cut-off threshold of $\epsilon \sim 0.008$ is installed, and is determine by the 99% confidence level of fluctuation in ϵ when the vesicle is in the relaxed spherical state. This change in the threshold results in only a 5% change in the values of κ and Γ_0 for this individual case. A similar approach is applied to all vesicles of POPC with 30% cholesterol, and the results are tabulated in Table S7. For all vesicles (except for #3), the change in κ is within 5% and the change in Γ_0 is within 7%. The M.E. remains essentially unchanged at 0.0023. In addition, if the same value of κ is assumed for all vesicles (Method B), we obtain $\kappa = 2.21 \times 10^{-19}$ J, which is only 1.4% different from that obtained with Method B in Table S5 (2.18×10^{-19} J). Taking together, we prefer the conservative threshold of $\epsilon = 0.015$ to manage noise contamination. Meanwhile, we do keep sufficient data for our quantitative analysis.

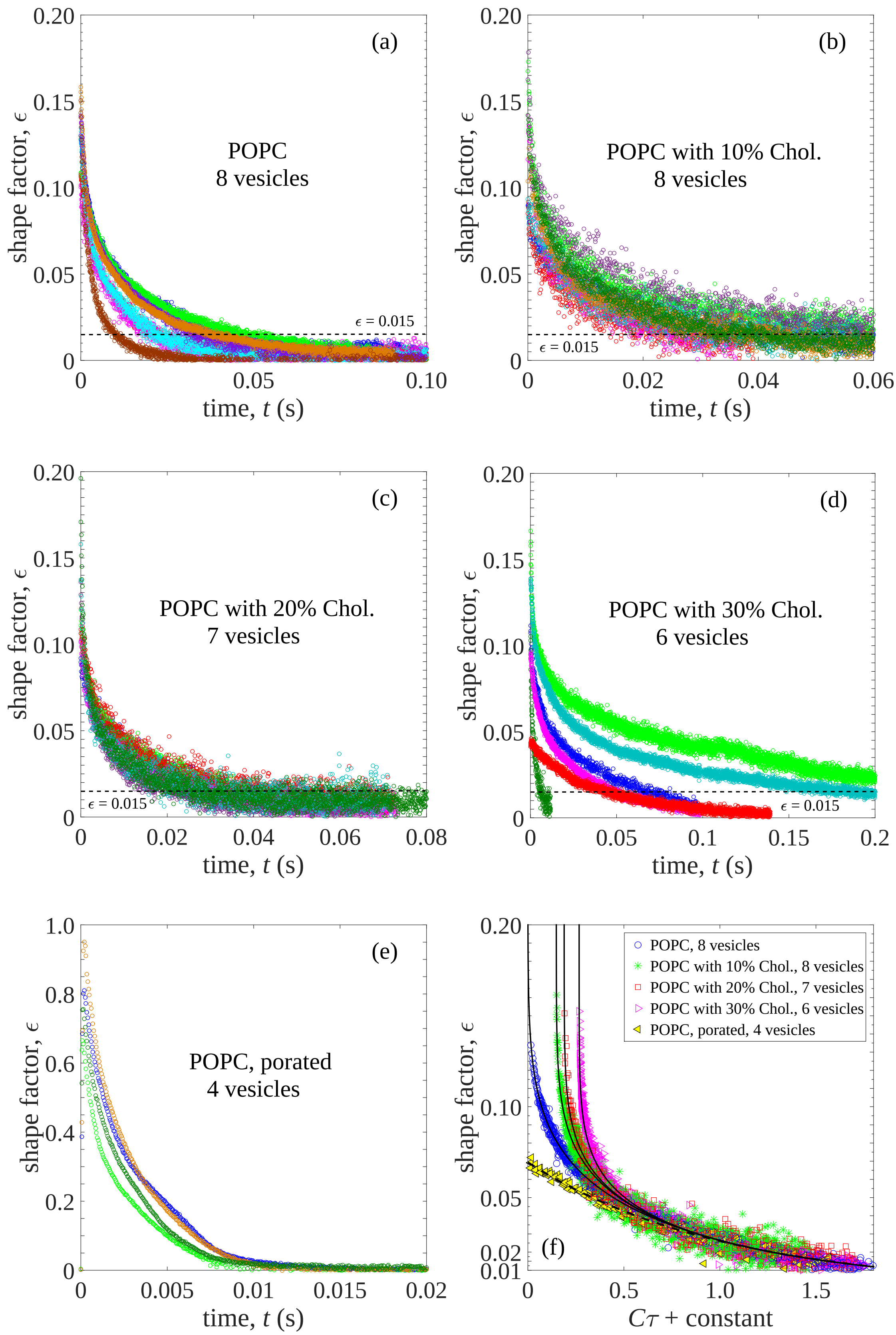

FIG. S5: (a)-(e) Data corresponding to Tables S2-S6. (f) Figure 3 of the main text, replotted on a linear scale for ϵ.

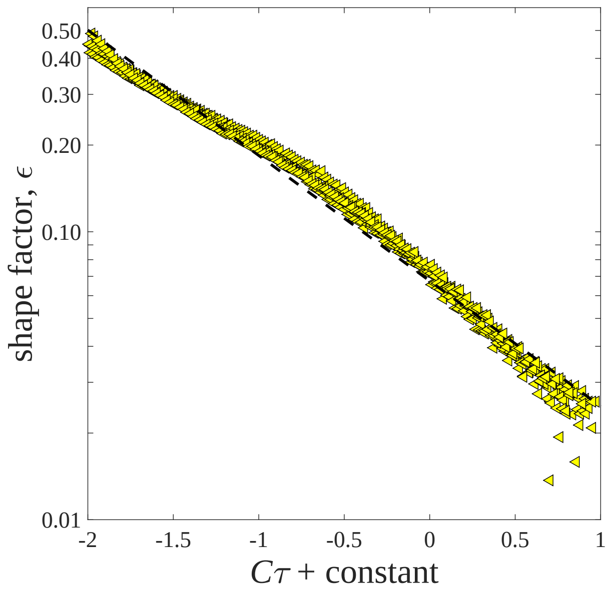

FIG. S6: Electroporated vesicles in Fig. 3 in the main text, replotted in a greater range of ϵ. The dashed line is a global fit for all 4 vesicles.

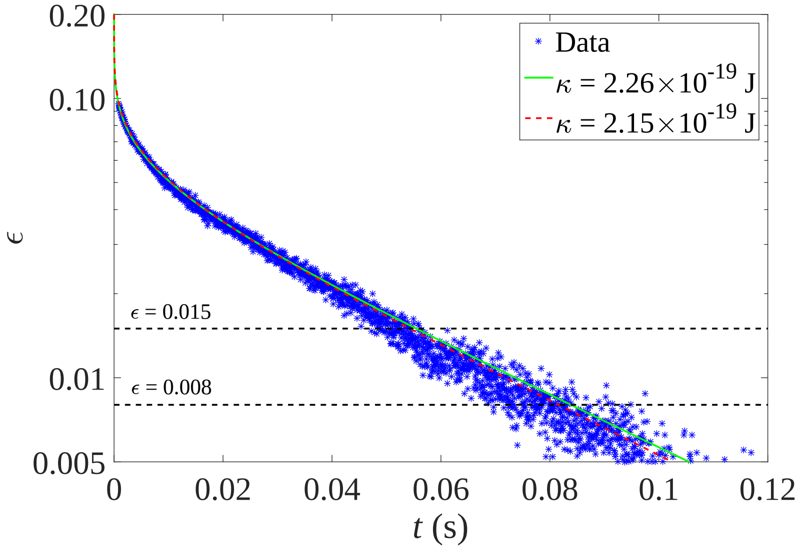

FIG. S7: Comparison between cut-off thresholds of $\epsilon = 0.015$ (solid) and $\epsilon = 0.008$ (dashed), for Vesicle #4, POPC with 30% cholesterol. The difference in the fitted κ-value is 5%.

		Method A			Method B		Method C		Pulse info.	
Parameter	r_0	κ	Γ_0	R^2	κ	Γ_0	κ	Γ_0	V_0	t_p
Unit	μm	10^{-19} J	10^{-6} N/m		10^{-19} J	10^{-6} N/m	10^{-19} J	10^{-6} N/m	V	μs
Vesicle #1	21.1	1.10	2.07	0.983	1.22	1.99	0.99	2.74	50	150
Vesicle #2	34.8	1.20	2.78	0.993	1.22	2.81	0.99	3.03	50	150
Vesicle #3	27.1	1.01	4.64	0.993	1.22	4.34	0.99	4.94	50	150
Vesicle #4	16.4	0.83	3.06	0.972	1.22	2.70	0.99	3.49	50	150
Vesicle #5	22.2	1.38	3.46	0.984	1.22	3.72	0.99	4.24	80	100
Vesicle #6	33.0	1.25	3.42	0.994	1.22	3.5	0.99	3.94	80	100
Vesicle #7	37.0	1.46	3.55	0.996	1.22	3.91	0.99	3.31	80	100
Vesicle #8	20.1	0.91	8.69	0.989	1.22	7.63	0.99	7.95	80	100
Average	26.5	1.14	3.96			3.83		4.21		
STD	7.68	0.22	2.05			1.71		1.67		
Mean error		0.0025			0.0027		0.0043			

TABLE S2: Parameters and results for the POPC data shown in Fig. 3. V_0 is the applied voltage, and t_p is pulse duration.

		Method A			Method B		Method C		Pulse info.	
Parameter	r_0	κ	Γ_0	R^2	κ	Γ_0	κ	Γ_0	V_0	t_p
Unit	μm	10^{-19} J	10^{-6} N/m		10^{-19} J	10^{-6} N/m	10^{-19} J	10^{-6} N/m	V	μs
Vesicle #1	18.0	2.76	1.34	0.911	1.73	1.76	1.77	1.83	80	150
Vesicle #2	18.0	1.75	1.12	0.951	1.73	1.12	1.77	0.88	80	200
Vesicle #3	15.9	2.86	1.71	0.815	1.73	2.18	1.77	1.79	50	200
Vesicle #4	15.9	1.77	1.94	0.939	1.73	2.02	1.77	2.49	50	250
Vesicle #5	15.9	1.72	1.45	0.868	1.73	1.45	1.77	1.02	80	100
Vesicle #6	15.9	1.66	0.79	0.946	1.73	0.74	1.77	0.71	80	150
Vesicle #7	19.1	1.84	1.75	0.952	1.73	1.86	1.77	1.9	50	200
Vesicle #8	19.1	1.41	1.87	0.972	1.73	1.64	1.77	1.93	80	100
Average	17.2	1.97	1.50			1.60		1.57		
STD	1.48	0.53	0.40			0.48		0.62		
Mean error		0.0051			0.0053		0.0065			

TABLE S3: Parameters and results for the POPC vesicles with 10% cholesterol shown in Fig. 3.

		Method A			Method B		Method C		Pulse info.	
Parameter	r_0	κ	Γ_0	R^2	κ	Γ_0	κ	Γ_0	V_0	t_p
Unit	μm	10^{-19} J	10^{-6} N/m		10^{-19} J	10^{-6} N/m	10^{-19} J	10^{-6} N/m	V	μs
Vesicle #1	23.0	1.72	2.10	0.971	1.90	1.99	2.22	2.26	50	150
Vesicle #2	23.0	1.91	1.90	0.977	1.90	1.90	2.22	2.11	50	200
Vesicle #3	18.2	1.89	1.38	0.946	1.90	1.38	2.22	1.28	50	150
Vesicle #4	20.7	2.53	2.16	0.961	1.90	2.60	2.22	1.90	50	150
Vesicle #5	20.7	1.86	3.57	0.971	1.90	3.57	2.22	2.59	50	200
Vesicle #6	20.7	2.62	2.20	0.917	1.90	2.80	2.22	2.12	50	250
Vesicle #7	20.7	1.63	3.22	0.961	1.90	2.81	2.22	2.78	50	300
Average	21.0	2.02	2.36			2.44		2.15		
STD	1.64	0.39	0.76			0.73		0.49		
Mean error		0.0039			0.0041		0.0056			

TABLE S4: Parameters and results for the POPC vesicles with 20% cholesterol shown in Fig. 3.

		Method A			Method B		Method C		Pulse info.	
Parameter	r_0	κ	Γ_0	R^2	κ	Γ_0	κ	Γ_0	V_0	t_p
Unit	μm	10^{-19} J	10^{-6} N/m		10^{-19} J	10^{-6} N/m	10^{-19} J	10^{-6} N/m	V	μs
Vesicle #1	27.1	2.21	1.18	0.985	2.18	1.18	1.91	1.41	50	100
Vesicle #2	27.1	2.17	0.26	0.981	2.18	0.26	1.91	0.33	80	100
Vesicle #3	37.6	2.07	2.04	0.982	2.18	1.98	1.91	2.15	50	50
Vesicle #4	37.6	2.26	2.21	0.982	2.18	2.27	1.91	2.52	50	100
Vesicle #5	37.6	2.24	0.65	0.988	2.18	0.65	1.91	0.64	80	100
Vesicle #6	21.6	1.94	15.3	0.954	2.18	14.6	1.91	15.0	50	100
Average	31.4	2.15	3.61			3.49		3.68		
STD	7.05	0.12	5.78			5.50		5.61		
Mean error		0.0023			0.0023		0.0030			

TABLE S5: Parameters and results for the POPC vesicles with 30% cholesterol shown in Fig. 3.

				Pulse info.	
Parameter	r_0	Γ_0	R^2	V_0	t_p
Unit	μm	10^{-6} N/m		V	μs
Vesicle #1	20.0	22.8	0.993	100	150
Vesicle #2	20.0	20.2	0.997	100	150
Vesicle #3	18.4	22.4	0.988	100	150
Vesicle #4	18.4	24.4	0.997	100	200
Average	19.2	22.5			
STD	0.92	1.73			
Mean error	0.0020				

TABLE S6: Parameters and results for porated POPC vesicles shown in Fig. 3.

Parameter	threshold	κ	Γ_0	threshold	κ	Γ_0
Unit		10^{-19} J	10^{-6} N/m		10^{-19} J	10^{-6} N/m
Vesicle #1	0.015	2.21	1.18	0.007	2.20	1.19
Vesicle #2	0.015	2.17	0.26	0.016	2.26	0.25
Vesicle #3	0.015	2.07	2.04	0.008	2.39	1.91
Vesicle #4	0.015	2.26	2.21	0.008	2.15	2.32
Vesicle #5	0.015	2.24	0.65	0.005	2.25	0.64
Vesicle #6	0.015	1.94	15.3	0.010	1.83	16.5
Average		2.15	3.61	0.009	2.18	3.80
STD		0.12	5.78	0.0034	0.17	5.72
Mean error		0.0023			0.0023	

TABLE S7: Comparison between fitting values of κ and Γ_0 with a global cut-off threshold ($\epsilon = 0.015$) and individual cutoff thresholds determined by 99% confidence level in the noise amplitude of ϵ when the vesicle is in a spherical state, for POPC vesicles with 30% cholesterol. Analysis follows Method A. Meanwhile, analysis with Method B reveals $\kappa = 2.18$ and 2.21×10^{-19} J, for the global and individual threshold, respectively.

[1] U. Seifert. Fluid membranes in hydrodynamic flow fields: Formalism and an application to fluctuating quasispherical vesicles in shear flow. *Eur. Phys. J. B*, 8:405–415, 1999.

[2] K. A. Riske and R. Dimova. Electro-deformation and poration of giant vesicles viewed with high temporal resolution. *Biophys. J.*, 88:1143–1155, 2005.

[3] P. F. Salipante and P. M. Vlahovska. Vesicle deformation in DC electric pulses. *Soft Matter*, 10:3386–3393, 2014.

[4] E. Evans and W. Rawicz. Entropy-driven tension and bending elasticity in condensed-fluid membranes. *Phys. Rev. Lett.*, 64:2094–2097, 1990.

[5] G. Niggemann, M. Kummrow, and W. Helfrich. The bending rigidity of phosphatidylcholine bilayers: dependences on experimental method, sample cell sealing and temperature. *J. Phys. II France*, 5:413–425, 1995.

[6] R. S. Gracia, N. Bezlyepkina, R. L. Knorr, R. Lipowsky, and R. Dimova. Effect of cholesterol on the rigidity of saturated and unsaturated membranes: fluctuation and electrodeformation analysis of giant vesicles. *Soft Matter*, 6:1472–1482, 2010.

[7] J. T. Schwalbe, P. M. Vlahovska, and M. J. Miksis. Vesicle electrohydrodynamics. *Phys. Rev. E*, 83:046309, 2011.

[8] S. Guido and M. Villone. Measurement of interfacial tension by drop retraction analysis. *J. Colloid Interface Sci.*, 209:247–250, 1999.

[9] M. I. Angelova and D. S. Dimitrov. Liposome electroformation. *Faraday Discuss. Chem. Soc.*, 81:303–311, 1986.

[10] K. A. Riske and R. Dimova. Electric pulses induce cylindrical deformations on giant vesicles in salt solutions. *Biophys. J.*, 91:1778–1786, 2006.

[11] R. C. Weast, editor. *Handbook of chemistry and physics.* CRC Press, 1988.

[12] M. M. Sadik, J. Li, J. W. Shan, D. I. Shreiber, and H. Lin. Vesicle deformation and poration under strong DC electric fields. *Phy. Rev. E.*, 83:066316, 2011.